Insular cortex to ventral striatum synapses encode valence of social interaction.

Pedro Espinosa[(1)], Benoit Girard[(1)], Mattia Lucchini[(1)], Federica Campanelli[(1)], Valentina Tiriticco[(1)] and Camilla Bellone[(1)] *

* Corresponding author: camilla.bellone@unige.ch

[(1)] University of Geneva, Department of Fundamental Neuroscience, CMU, 1 rue Michel-Servet, 1211, Geneva (Switzerland).

Abstract

The decision to approach or avoid a conspecific is fundamental for survival. Affiliative (prosocial) interactions favor approach behaviors, while antagonistic (aggressive) contacts trigger avoidance. Here we ask how the brain encodes the valence of social interaction. We focused on the nucleus accumbens (NAc), a brain region implicated in social reward processing. We observed that social interactions activate D1-expressing medium spiny neurons (D1-MSNs) regardless of their valence. However, afferent D1-expressing neurons of the anterior insular cortex (AIC) exhibited distinct activity patterns coding for prosocial and aggressive social interaction, respectively. As a result, distinct forms of synaptic plasticity were elicited at the AIC to NAc synapses. Thus, the valence of social interaction induces distinct neural activity in the AIC, which teaches the animal to approach and avoid conspecifics in the future.

Main

Even though many interactions with conspecifics are rewarding, only some are positive experiences. It is essential for individuals of all species to identify and distinguish prosocial from aversive interactions to determine whether to approach or avoid their conspecific in the future. In this context, social valence refers to the degree to which an experience with a conspecific is pleasurable (positive) or aversive (negative)[1]. Several studies have investigated the role of different brain circuits in social behavior[2–5]. Still, it has yet to be determined if there are specific brain networks with mechanisms that favor valence attribution in a social context.

The mesolimbic system has been implicated in interactions between conspecifics of the same sex[3,4,6,7]. This system originates in the Ventral tegmental area (VTA), where Dopamine (DA) neurons project mainly into Nucleus Accumbens (NAc). Although the canonical view in the field postulates that D1-expressing Medium Spiny Neurons (MSNs) integrate rewarding signals, emerging evidence indicates that these neurons modulate also aversive experiences[8,9,10]. Indeed, stimulation of D1-MSNs increases the time spent in the interaction between two sex-matched mice[2], while bidirectional modulation of the activity of these neurons during an aggressive interaction is associated with the emergence of a susceptible phenotype after defeat[11]. Here we investigate how D1-MSNs compute prosocial and aggressive interactions and allow behavioral adaptations based on social valence.

D1-MSNs from Lateral NAc encode social proximity but not social valence.

To mimic prosocial and aversive social experiences, we exposed experimental adult male mice to unfamiliar sex-matched stimuli (juvenile C57BL/6J or adult aggressive CD1) for 15 min of free direct social interaction. We used the inanimate object as a non-social experience (Fig. 1a). We observed that experimental mice engaged in a high number of prosocial interactions (reciprocal and approach behaviors; Fig.1b) and spent most of the time in the proximity of the juvenile conspecifics (Fig. 1c). However, when confronted with CD1 stimuli, mice engaged in antagonistic interactions (avoidance and aggressed behaviors; Fig. 1b) and tended to stay distant from them most of the time (Fig. 1c). Interestingly, animals exposed to prosocial experiences spent more time in the frontal field of the experimental mice (Fig. 1d). Conversely when exposed to aversive stimuli, mice had higher velocity when CD1 stimuli were behind them (Fig. 1e). According to these results, interactions with juvenile or CD1 stimuli are characterized by distinct behavioral responses.

To study how D1R-containing MSNs compute social valence, we focused on the lateral portion of the NAc shell (LNAc). Indeed, the NAc subdivisions can oppositely influence

motivated behavior [12], and the lateral part has been associated with rewarding and aversive experiences[13]. Using a miniscope, we recorded the calcium activity of individual neurons from LNAc D1-MSNs during the prosocial and aversive experiences (Fig. 1f). Overall, calcium transients increased in both conditions. Still, no change in activity was revealed during the non-social experience (Fig. 1g). Additionally, we observed that the calcium activity increased when the social stimuli were near the experimental mouse regardless of their identity (Fig. 1h,i) and that 71.6% of neurons showed increased activity during both prosocial and aversive experiences (Fig. 1j). The results suggest that LNAc D1-MSNs encode conspecific proximity independent of valence.

D1-containing neurons of the Anterior Insular Cortex project to LNAc.

We employed a neural activity-dependent labeling approach to investigate which inputs promote D1-MSN activity during prosocial and aversive experiences. Specifically, we injected Fos-cre-ER^{T2} mice in the LNAc with a retro-AAV-FLEX-tdTomato virus to target the inputs involved in social interaction. Four weeks after the injection, we exposed mice to non-social, prosocial, or aversive experiences for 15 min followed by tamoxifen administration to target the active projections (Extended data Fig. 1a-b). We identified neurons activated by prosocial and aggressive experiences in different rostrocaudal subdivisions of the Insular cortex (anterior insular cortex-AIC, medial Insular Cortex- mIC and posterior Insular Cortex-pIC) and amygdala (Extended data Fig. 1b,c).

The insular cortex has an integrative function, plays an essential role in salience processing and attention, and gates executive control[1415]. All these functions are involved in social behavior and valence processing.

By injecting a retrograde rabies virus into the LNAc, we found that only the anterior section of the insula projects monosynaptically to the D1-MSNs in the lateral part (Extended Data Fig. 2a-e). To determine the identity of the socially active neurons in the AIC that project to the LNAc, RNA scope in situ hybridization was used to double label Fos and Drd1 mRNA[16]. We observed that 88,16% of juvenile-activated neurons and 81.4% of CD1-activated neurons were Drd1 positive (Extended data Fig. 3a,b). We confirmed these results using a bicolor virus approach and injecting AAVrg-ef1a-DO-DIOTdTomato-eGFP in the LNAc and labeling neurons in the AIC (Extended data Fig. 3c,d). According to these data, despite D1 positive and D1 negative neurons project to the LNAc, most neurons activated by prosocial and aversive experiences contained D1Rs.

The activity of D1-AIC neurons projecting to LNAc predicts social valence.

Next, we examined the role of D1-AIC to LNAc pathway during prosocial and aggressive experiences using miniscope (Fig. 2a). A general increase in calcium activity was observed

in D1-AIC neurons projecting to LNAc when mice were exposed to juveniles and CD1 stimuli (Fig. 2b). The next step was to determine whether specific neurons were activated during prosocial or aversive experiences and whether stimulus proximity drives ensemble activation. Our analysis revealed that only 46.6% of neurons were activated in both conditions (Fig. 2e) and that compared to D1-MSNs in the LNAc, the increase in activity was not related to proximity (Fig. 2c-d).

To reveal whether the AIC to LNAc pathway was involved in social interactions, we develop an unsupervised deep learning approach to classify each contact with a conspecific as affiliative or antagonistic and therefore determine the valence of prosocial and aversive experiences from the activity of D1-AIC neurons projecting to LNAc. Based on the pose dynamics obtained from Deeplabcut[17], we trained a Variational Autoencoder (VAE) based on the prosocial contacts and then produced a latent embedding of all the contacts with conspecific observed during prosocial and aversive experiences. We then used this latent representation to build a behavioral classifier (SVM) that predicts the nature of the experience (Fig. 2f, and Extended figure 6; accuracy of 89.9% for prosocial and 68,1% for aversive experience (Fig.2g)). To validate our approach, we compared the behavioral classifier with independent human manual annotations. The contacts detected by the behavioral classifier were then defined as affiliative or antagonistic and matched with manual annotation of prosocial (nose-nose) and aggressive (attack) interactions (Fig. 2g).

Finally, we extracted features from the calcium activity recorded (Extended figure 7) and built a neuronal classifier (K-Nearest Neighbors -KNN) to predict affiliative or antagonistic contacts identified by the behavioral classifier (Extended figure 7). Strikingly, calcium activity recorded during prosocial experience has a higher prediction score for affiliative than antagonistic contacts. At the same time, calcium activity recorded during aversive experience has a higher prediction score for antagonistic compared to affiliative contacts (Fig. 2h). According to these data, calcium activity in D1-AIC neurons projecting to LNAc can be used to decode the valence of social contact.

The AIC-NAc synapses exhibited distinct synaptic plasticity during prosocial and aggressive interactions.

We next hypothesized that an activity-dependent modulation of the strength of AIC to LNAc inputs during prosocial and aggressive interactions might contribute to regulating approach or avoidance behavior. To test our hypothesis, we first verified the specificity of the projection from D1-containing AIC neurons to D1-MSNs in the LNAc. We injected AAV-FLEX-ChR2 in AIC and AAV-FLEX-mCherry in the LNAc in D1-Cre mice and performed double whole cell patch clamp recording from labeled D1 positive and D1 negative neurons in the LNAc (Fig. 3a). We showed that D1-expressing AIC neurons were preferentially

projecting to D1-MSN in the LNAc, revealing a novel D1-D1 top-down circuit between AIC and LNAc (Fig. 3b-c).

To investigate whether prosocial and aversive experiences induce forms of synaptic plasticity at AIC to LNAc synapses, 24 hrs after stimuli exposure we performed whole-cell recording from D1-MSNs in the LNAc while recording excitatory inputs from the D1-containing AIC neurons (Fig. 3d). We measured the relative ratio of AMPAR to NMDAR mediated currents (AMPA/NMDA ratio) as a proxy of synaptic strength and rectification index of AMPARs as a proxy of the proportion of calcium-permeable receptors (CP-AMPARs) recruited at these synapses [18,19]. We observed an increase in AMPA/NMDA ratio after prosocial and an increase in the rectification index after the aversive experience (Fig. 3e-f), supporting the hypothesis that social valence drives different forms of synaptic plasticity at AIC to LNAc synapses exclusively in D1 receptor-expressing neurons (Extended Figure 8).
Since we have shown that social valence could be decoded from the calcium activity of D1-AIC neurons projecting to the LNAc, we hypothesize that valence-dependent synaptic plasticity results from different activity patterns at AIC-LNAc pathway during prosocial and aggressive interactions (Extended Figure 9).To test our hypothesis, we injected AAV-FLEX-ChR2 in the AIC in D1-Cre mice, AAV-FLEX-mCherry in the NAc and implanted optic fibers in the LNAc bilaterally (Fig. 3g). We stimulated the AIC to LNAc pathway at low (1 Hz) or medium (10 Hz) frequency while stimulating the contralateral hemisphere with 0.1 Hz. Then, 24 hrs after the optogenetic stimulation, we performed whole cell patch clamp recording from D1-MSNs in the NAc and observed an increase in AMPA/NMDA ratio following low stimulation and an increase in rectification index after medium stimulation (Fig. 3h-i). As concluded by these data, prosocial and aversive experiences produce different patterns of activity at the AIC and LNAc. Thus, distinct forms of plasticity are elicited.

Valence-dependent synaptic plasticity is required for learned approach behavior

In the next step, we tested the hypothesis that valence-dependent synaptic plasticity at AIC to LNAc synapses contributes to social behavioral adaptations. On the first day we exposed the experimental mice to prosocial or aversive experiences. On day 2, we examined the mice on the approach/avoidance test (Fig. 4a). Mice freely explored an open arena containing an empty enclosure during the pre-test. As part of the test phase, we placed in the enclosure the stimulus they were exposed to on day 1 and measured the proximity and time between them. We observed that experimental mice approached the juvenile while avoiding the CD1 stimuli (Fig. 4b), indicating that mice learn to approach or avoid conspecific based on the previous interaction.

To test the causality between behavior, synaptic plasticity, and activity pattern, we exposed experimental mice to prosocial interaction. We delivered 10Hz stimulation at AIC to LNAc pathway during affiliative contacts throughout the prosocial experience (Fig. 4c-d) to mimic the antagonistic-dependent synaptic plasticity. On day 2, we completed the approach/avoidance test and performed whole cell patch clamp recording of D1-MSN in the LNAc while stimulating AIC inputs. We observed that while control mice approached juvenile stimuli during the test phase, the approach behavior was abolished in mice exposed to prosocial experience and medium-frequency stimulation during the affiliative contacts (Fig. 4e-f). On the very same mice, we then performed electrophysiological recording from D1-MSNs while recording EPSC from AIC inputs. We observed a difference in AMPA/NMDA ratio between groups of mice. Specifically, the AMPA/NMDA ratio recorded after prosocial interaction was higher than the ratio recorded in mice where affiliative contacts were coupled with 10 Hz (Fig.4g). Interestingly, we observed a linear correlation between the rectification index and avoidance index: the higher the proportion of GluA2-lacking AMPARs at the AIC-LNAc synapses, the higher the avoidance behavior toward juvenile stimulus (Fig. 4h-i).

Our results reveal novel social valence-dependent forms of synaptic plasticity between D1-AIC to D1-LNAc. This plasticity constitutes the neuronal substrate for learned approach behavior. Interestingly, these forms of plasticity arise from specific activity patterns in this pathway, defining a distinct signature for social valence. It is also important to note that valence is more than the activation or inhibition of a specific neuronal subpopulation according to the canonical definition. Our data indicate that valence is determined by the pattern of activity and the subsequent experience-dependent synaptic changes that drive learned behaviors.

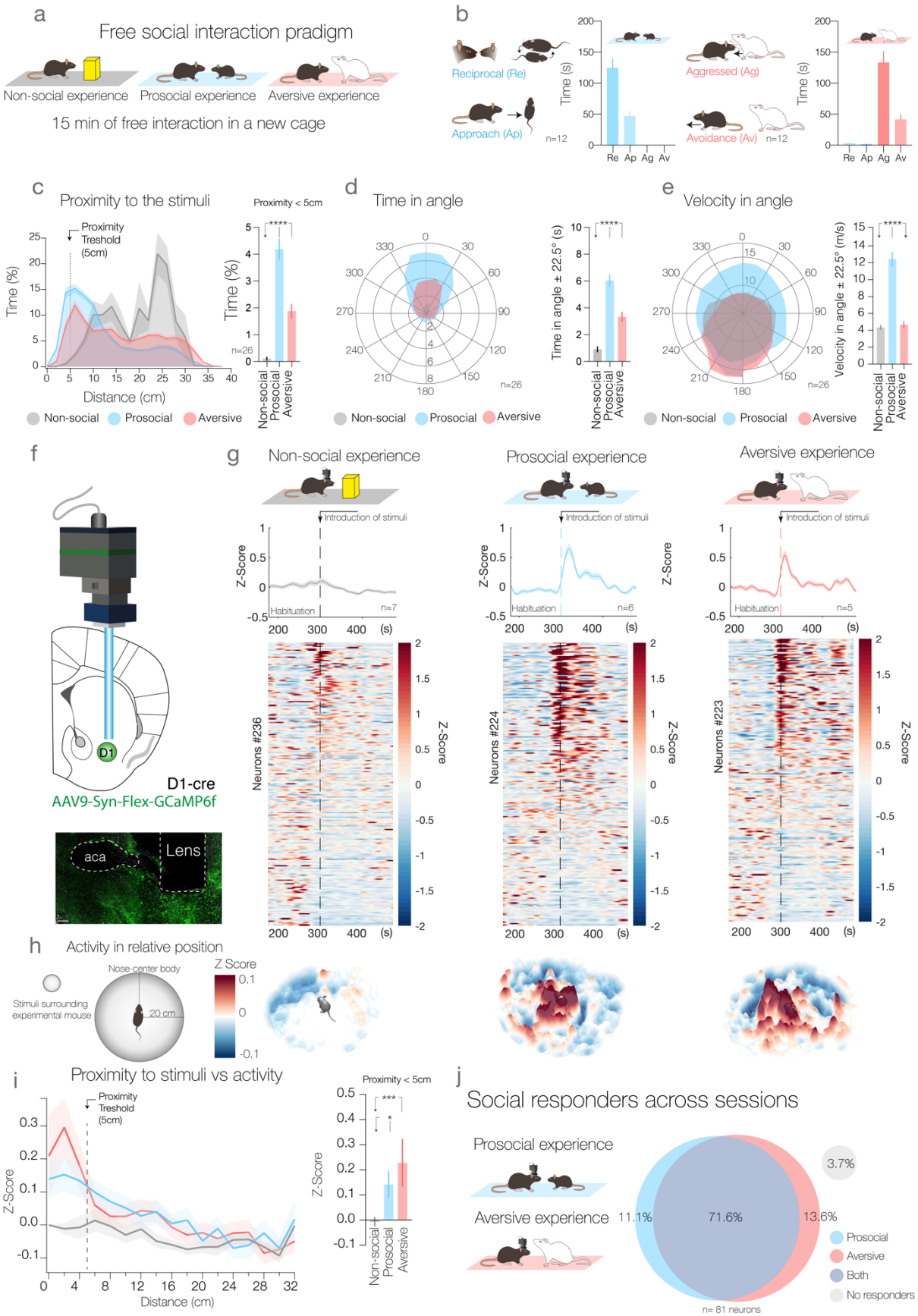

Figure 1. D1-MSNs encode for proximity to social stimuli, independent of the valence of the experience. a, Schematic representation of behavioral paradigms. **b**, Schema and time

spent in manually scored events. **c**, Linear plot representing the % of Time as a function of the distance between the experimental mouse and the stimulus. Right, bar plot showing the percentage of time spent in proximity (<5 cm), ****=p < 0.0001. **d**, Polar Plot representing the Time in angle. Right, quantification between ±22.5 degrees of the polar plot, ****=p < 0.0001. **e**, Polar Plot representing velocity peak. Right, quantification between ±22.5 degrees of the polar plot, ****=p < 0.0001. **f**, Schematic of viral injection and GRIND lens implantation. Below: representative image of the site of injection and implantation, scale 150um. **g**, Time course of the overall normalized calcium activity. Below: the associated heatmap of each neuron. **h**, Schema and 3D heat map of the overall normalized calcium activity of D1-MSNs depending on the relative position of the social stimulus. **i**, Left: Lineal plot representing the normalized calcium activity in function of the distance between the experimental mouse and the stimulus. Right, bar graph representing the quantification of activity in proximity (<5 cm), ***p=0.0005, *=0.0432, n=81 (prosocial and aversive) and n=236 for the object. **j**, Percentage of neurons responding to stimulus across sessions. One-way ANOVA was used for the statistical test. n denotes the number of mice in each group. Data are shown as mean, and error bars represent s.e.m.

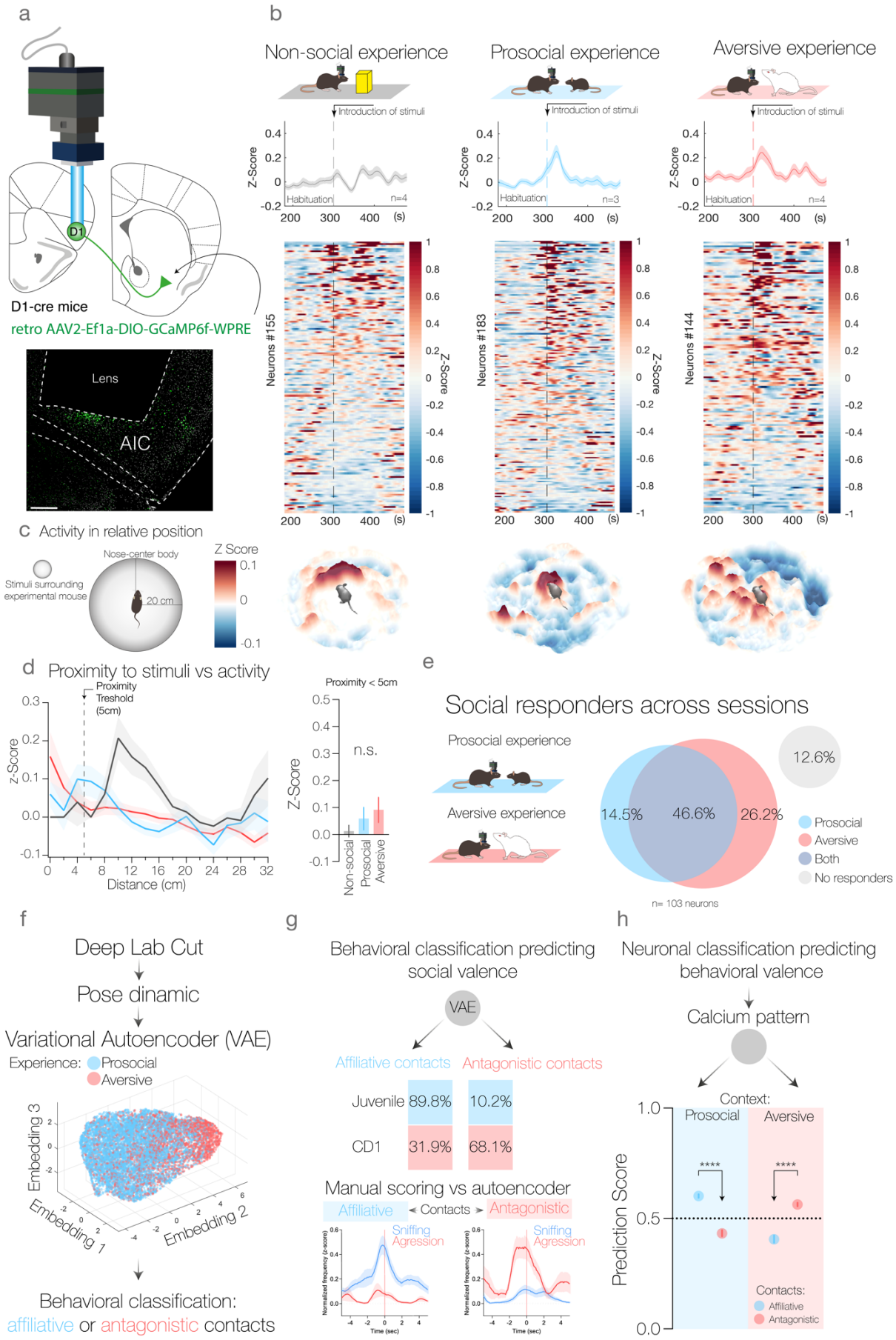
a
D1
D1-cre mice
retro AAV2-Ef1a-DIO-GCaMP6f-WPRE
Lens
AIC
b
Non-social experience
Prosocial experience
Aversive experience
Introduction of stimuli
Z-Score
Habituation
n=4
n=3
n=4
Neurons #155
Neurons #183
Neurons #144
c Activity in relative position
Stimuli surrounding experimental mouse
Nose-center body
20 cm
Z Score
d Proximity to stimuli vs activity
Proximity Treshold (5cm)
z-Score
Distance (cm)
Proximity < 5cm
n.s.
Non-social
Prosocial
Aversive
e
Social responders across sessions
Prosocial experience
Aversive experience
14.5%
46.6%
26.2%
12.6%
Prosocial
Aversive
Both
No responders
n= 103 neurons
f
Deep Lab Cut
Pose dinamic
Variational Autoencoder (VAE)
Experience: Prosocial
Aversive
Embedding 3
Embedding 1
Embedding 2
Behavioral classification:
affiliative or antagonistic contacts
g
Behavioral classification predicting social valence
VAE
Affiliative contacts
Antagonistic contacts
Juvenile 89.8% 10.2%
CD1 31.9% 68.1%
Manual scoring vs autoencoder
Affiliative
Contacts
Antagonistic
Sniffing
Agression
Time (sec)
h
Neuronal classification predicting behavioral valence
Calcium pattern
Context:
Prosocial
Aversive
Prediction Score
Contacts:
Affiliative
Antagonistic

Figure 2. D1R-AIC neurons predicts social valence. a, Top: Schematic representation of viral injection and baseplated GRIND lens implantation. Below: representative image of site of injection and implantation, scale 250 um. **b**, Timecourse of the overall normalized calcium activity recorded with miniscope. Top: Averaged activity of the overall population. Below: associated heatmap of each individual neurons. **c**, Heatmap of relative position in function of activity, showing no correlation between activity and proximity space for prosocial, aversive or non-social experiences.. **d**, Linear plot representing the normalized calcium activity in function of the distance between the experimental mouse and the stimulus. Right, quantification of activity during approaching bouts (<5 cm). **e**, Percentage of neurons responding to stimulus across sessions. **f**, Pipeline of the model that represent and classify social contact as affiliative or antagonistic. **g**, Top, high accuracy of prediction of contacts from prosocial and aversive experiences. Below, the contacts defined as affiliative or antagonistic match with human manual scoring. **h**, Activity pattern extracted from calcium activity of D1R-AIC neurons during prosocial or aversive experience predict with high accuracy the predominant contact (affiliative or antagonistic). For affiliative contacts we used 613 trials, and for antagonistic contacts 618 trials, ****=$p < 0.0001$. One-way ANOVA was used in d, and Kruskal-Wallis test was used in h. n denotes the number of mice in each group. Data are shown as mean and error bars represent s.e.m., n.s. = non statistically significant.

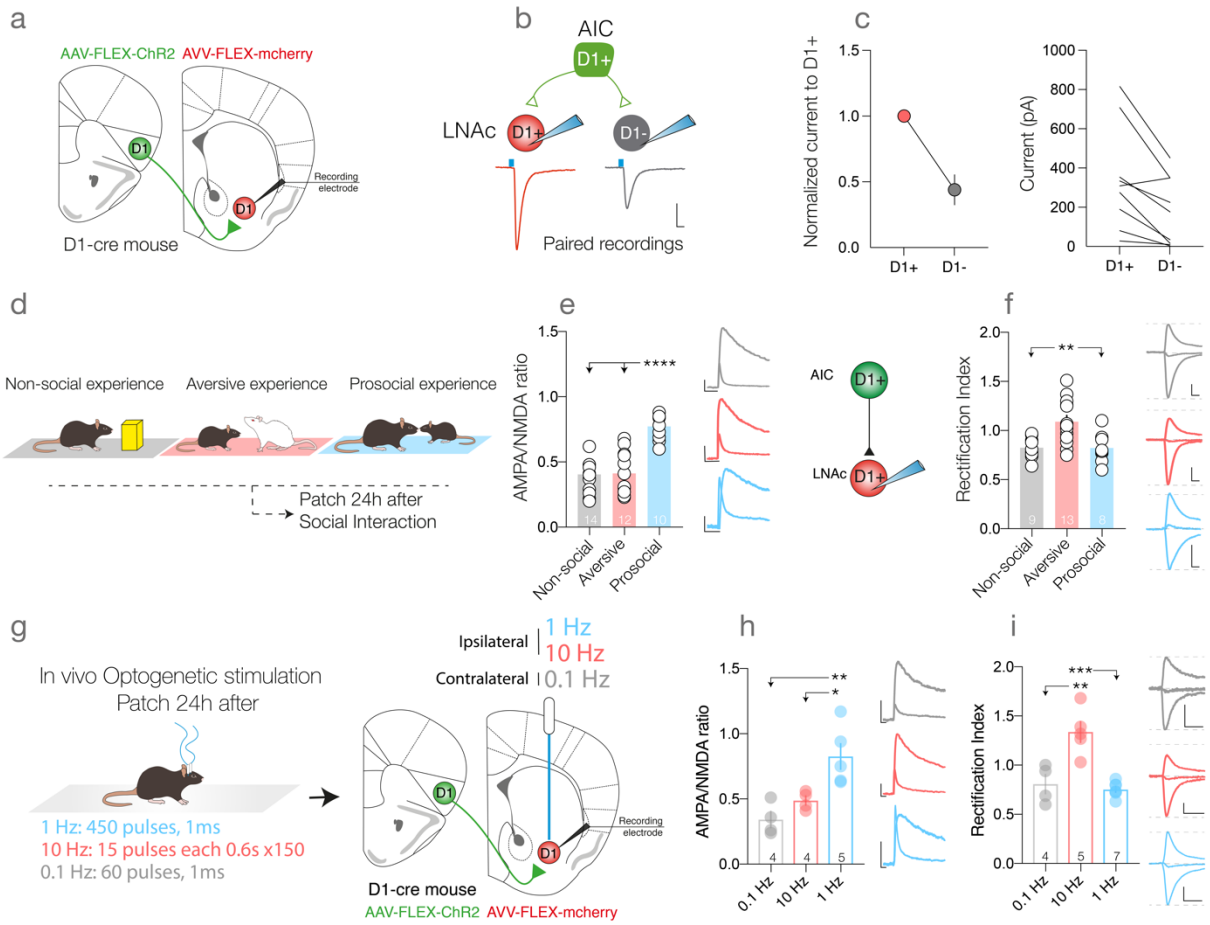

Figure 3. Social valence induce specific long-term synaptic plasticity in AIC-LNAc pathway a. Schematic of viral injection into LNAc and AIC. **b**. Schematic and representative trace of pairing recording between D1+ and D1- MSN in the LNAc. **c**. The graph shows the normalized current (left) and the net current for each pair of cells (right). **d**. Schematic representation of the behavioral paradigm. **e**. Bar graph representing the AMPA/NMDA ratio 24h after the behavioural experiment Right, example traces, ****=p < 0.0001. **f**. Bar graph representing rectification index 24h after free interaction. Right, example traces **= p=0.0094 for Aversive vs Prosocial and **=p = 0.0077 for Aversive vs object, **g**. Schematic of in vivo stimulation protocol. **h**, Bar graph representing the AMPA/NMDA ratio 24h after optogenetic stimulation. Right, example traces, **=p = 0.0036, *=p = 0.0292. **i**. Bar graph representing the rectification index Right, example traces, **=p = 0.0011, ***=p = 0.0001. One-way ANOVA was used as statistical test. Numbers inside bars denotes the number of cells in each group. Data are shown as mean and error bars represent s.e.m. Scales 50pA/10ms.

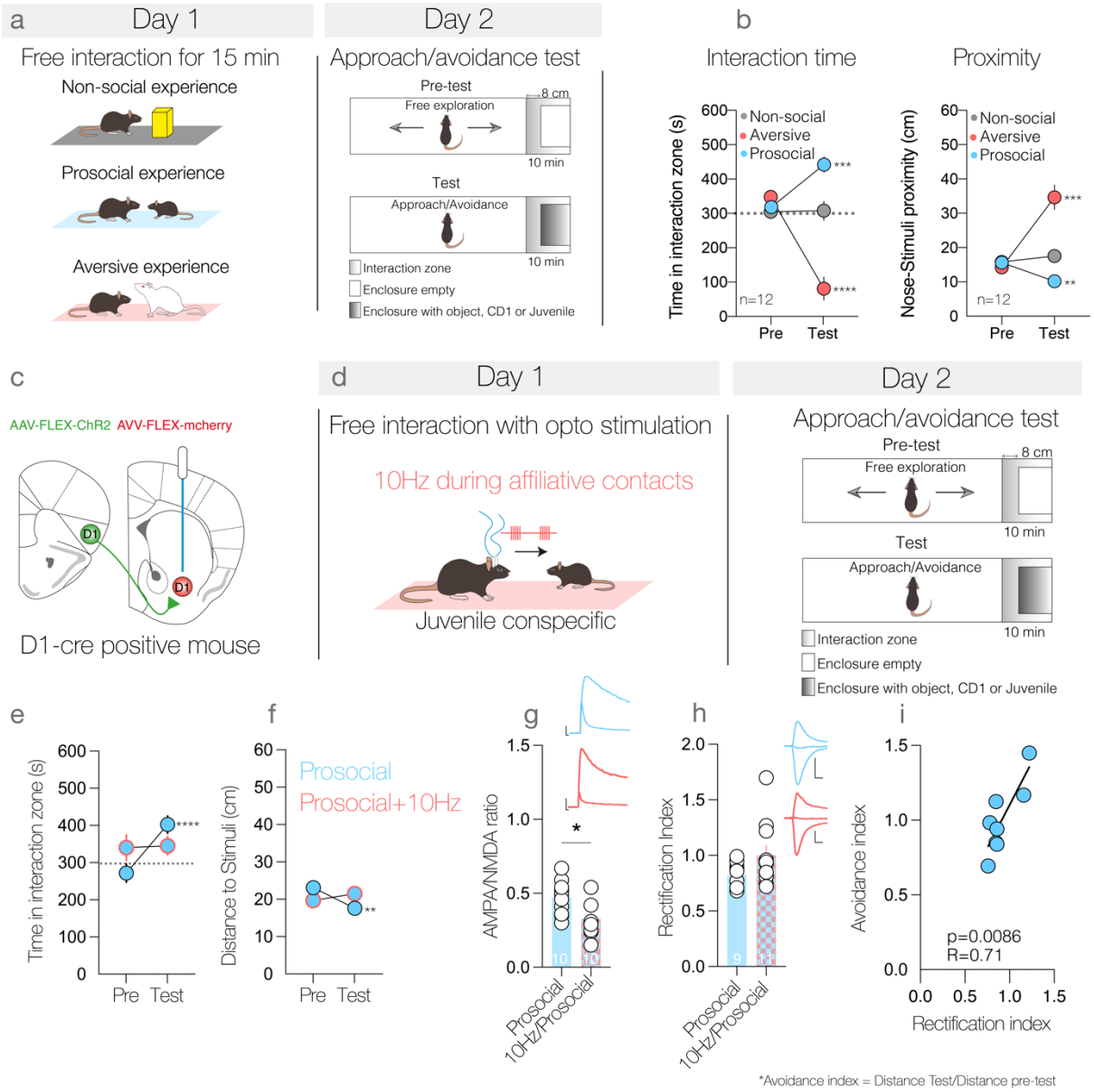

Figure 4. Valence-dependent synaptic plasticity is required for learned approach behavior a. Schematic of free interaction protocol (day 1) and approach/avoidance test (day 2). **b.** Appetitive and aversive stimuli have opposite effects on interaction behavior on day 2. Graph showing the interaction time during the pre-test and test for each stimulus, ***= p=0.0002, ****=p < 0.0001 and p=0.9130 for object. Right, plot showing the proximity between the nose point and the center of the enclosure, **= p=0.0013, ***= p=0.0001 and p=0.3020 for object. **c**. Schematic of the viral injection site and fiber implantation. **d**. Schematic of the protocol **e**. Graph showing time in interaction zone, ****= p= < 0.0001 and p=0.8745 for Prosocial **f**, Graph showing distance to stimuli, **= p=0.0027 and p=0.4030 for Prosocial **g**, Bar graph representing AMPA/NMDA ratio, *= p=0.020. **h**, Bar graph representing rectification index, p=0.1048. **i**, Correlation between the rectification index and the avoidance index. The avoidance index corresponds to the distance during post-test divided by distance during pre-test, p=0.0086 and R square= 0.71 (each dot represents one single animal, n=8). Paired t-test was used in b, e and f. Unpaired t-test was used in g and h. Numbers inside bars denotes the number of cells in each group. Data are shown as mean and error bars represent s.e.m. Scales 50pA/10ms.

Material and methods

Animals

The study was conducted with WT and transgenic mice in C57BL/6J background. For D1 neuron-specific manipulations D1-Cre (Tg(D2d1a-cre)EY262 Gast) mice from Charles River were used. Concerning expression mediated staining CreERt2 (Fos<tm2.1(icre/ERT2)Luo>) mice were used (in-house breed). An additional line referred to as CD1 (Crl:CD1(ICR)) was used for stimuli involved in aggressive behaviors, they were obtained from Charles Rivers. CD1 stimuli correspond to retired breeders more than 4 months old and they were screened for aggressiveness according to Golden et al. 2011.

All the animals were grouped housed (2-5 per cage) and stayed with the same cage mates since they were weaned (P21 - P28). They stayed under a 12 h light – dark cycle (7:00 a.m.–7:00 p.m.). All physiology and behavior experiments were performed during the light cycle. All the procedures were performed at UNIGE complied with the Swiss National Institutional Guidelines on Animal Experimentation and were approved by the Geneva Cantonal Veterinary Office Committees for Animal Experimentation.

Surgeries

For all the surgical procedures described hereafter, mice were anesthetized with a mixture of oxygen (1 L/min) and isoflurane 2% (Baxter AG, Vienna, Austria) and placed in a stereotactic frame (Angle One; Leica, Germany). The skin was locally anesthetized with 40–50 µL lidocaine 0.5% and disinfected with betadine.

Fos CreERt2 mice:
Injections of AAVrg-Flex-tdTomato (retrograde virus) were performed in male CreERt2 mice at 17 weeks of age. Unilateral craniotomy (1 mm in diameter) was then performed over the lateral shell of the NAc at the following stereotactic coordinates: AP + 0.9 mm, ML ± 1.9 mm, DV −4.0 mm from Bregma. The virus was injected via a glass micropipette (Drummond Scientific Company, Broomall, PA) into the lateral shell of the NAc for a total volume of 200 nL. The virus was incubated for 4 weeks prior to perform the behavioural tasks.

Biocolor:
Injections of AAVrg-ef1a-DO-DIO-TdTomato-eGFP were performed on D1-Cre male and female mice at 6-12 weeks. Unilateral craniotomy was performed over the lateral shell (AP

+ 0.9 mm, ML ±1.9 mm, DV −4.0 mm from Bregma). The volume of virus injected was 150 nL. The virus was incubated for 4-5 weeks prior to perform the perfusion and acquisition of the images.

In-vivo calcium imaging:

Injections of AAV-Flex-GCamp6f for LNAc recordings and AAV-Flex-GCamp6f retrograde for AIC recordings were performed in male D1-cre mice. Unilateral craniotomy (1 mm in diameter) was then performed over the lateral shell of the NAc at the following stereotactic coordinates: AP + 0.9 mm, ML ± 1.9 mm, DV −4.0 mm from Bregma. The virus was injected via a glass micropipette (Drummond Scientific Company, Broomall, PA) into the lateral shell of the NAc for a total volume of 300 nL. The virus was incubated for 3 weeks prior the implantation of the GRIND lens 0.6mm diameter and 7.3mm long at LNAc AP + 0.9 mm, ML ± 1.9 mm, DV −4.0 mm from Bregma. For AIC: GRIND lens 1mm diameter and 4mm long at AP + 2.15 mm, ML ±2.25 mm, DV −2.0 mm from Bregma were used.

Patch clamp:

Injections were performed on D1-Cre male mice at 6-11 weeks. Bilateral craniotomy was performed over the lateral shell (AP + 0.9 mm, ML ±1.9 mm, DV −4.0 mm from Bregma) injecting AAV-DIO-mCherry and over the AIC (AP + 2.15 mm, ML ±2.25 mm, DV −2.0 mm from Bregma) injecting AAV-Syn-DIO-ChR2-eGFP or AAV-Syn-DIO-ChR2-mCherry. The volume of virus injected was 200 nL. The virus was incubated for 4-5 weeks prior to perform the experiments.

In-vivo stimulation:

The same surgery as described before for patch clamp animals. The virus was incubated for 3 weeks prior to implanting the optic fiber. A bilateral craniotomy was performed over the lateral shell (AP + 0.9 mm, ML ±1.9 mm, DV −4.0 mm from Bregma) placing two optic fiber (250µm diameter), we cemented them with C&B-Metabond® and dental acrylic cement. After two weeks of recovery, we performed the experiments.

Rabies:

Injections of AAV8-hSyn-Flex-TVA-P2A-GFP-2A-oG were performed on D1-Cre male and female mice at 8-10 weeks over the lateral shell (AP + 0.9 mm, ML ± 1.9 mm, DV −4.0 mm from Bregma). After an incubation period of 4-5 weeks mice were injected at the same coordinates with EnvA-RVdG-mCherry. The volume injected in each procedure was 150 nL. The virus was incubated for 1 week after the last injection prior to performing anatomical experiments.

Anatomy

Anatomical tracing of active inputs using CreRT2 animals

After the free social interaction test previously described, we wait 4 weeks for the expression of the virus. Then, the animals were sacrificed by lethal injection of pentobarbital and transcardially perfused with phosphate buffer solution (PBS) 1x followed by 4% paraformaldehyde prepared in PBS 1x. The brain was then extracted and stored at 4°C overnight to postfixate in the same solution. The relevant regions of the brain were sliced in 50 µm thick coronal slices (Leica VT1000 S). Then the slices were mounted and covered with mounting medium with DAPI and cover slides.

CreERt2 mice cell counting

Following a qualitative analysis of the viral expression only a subset of regions was taken into consideration for quantitative cell counting; these regions being: pyriform cortex (Pyr), basolateral amygdala (Amy), paraventricular nucleus of the thalamus (PVT) and the insular cortex divided into 3 rostro-caudal segments (anterior insular cortex (AIC), medial insular cortex (mIC) and posterior insular cortex (pIC)).

Image processing and cell counting were performed using Zen 3 (Blue version) software using built-in cell counting and regions of interest (ROI) measurements features. Structural boundaries of the abovementioned regions were identified with anatomical landmarks according to a brain atlas (Franklin & Paxinos, 2008).

For each region positive cells and area were measured. Density index was then calculated in Excel by dividing positive cells of each structure by its area (in square mm). Every region was counted a similar number of times on different slices by two independent experimenters. Individual data were then pulled together and analysed using GraphPad Prism 7.

Representative photos of CreERt2 mice

For representative photos of Crert2 mice, we did an immunohistochemistry against td-Tomato. We incubated 48h at 4°C with rat anti-tdTomato (16D7, Kerafast) diluted 1:500 in a solution of 3% bovine albumin serum and 0.3% Triton X-100 prepared in PBS 1x. After primary incubation, the tissue was rinsed 3 times with PBS 1x and incubated at room temperature for 1.5h with donkey anti-rat IgG H&L (Alexa Fluor® 555) diluted 1:500 in a solution of 0.25% Tween- 20 prepared in PBS 1x.

Bicolor cell counting

Images were acquired with an LSM700 confocal microscope, LSM 800 Airyscan confocal microscope or Axioscan-Z1 epifluorescence slide scanner. Only images captured with the Axioscan-Z1 without immunohistochemistry were used for cell counting. Image processing was performed using Zen 2 (Blue version) software. Cell counting and area measurements were performed with Fiji-ImageJ software using built-in cell counting and regions of interest (ROI) measurements features. ROI and approximated distance from Bregma were identified with anatomical landmarks according to a brain atlas (Franklin & Paxinos, 2008). For mice infected with AAVrg-ef1a-DO-DIO-TdTomato-eGFP the area of the IC as well as the number of Cre positive and Cre negative insular projecting neurons were counted following a rostrocaudal gradient ranging between +2.50 mm and -0.50 mm from the Bregma. Cellular density was then calculated using number of cells over the area of the IC expressed in mm^2. Individual measurements were averaged and clustered in 6 segments of 0.5mm (ranging from +2.25 to -0.25 mm from Bregma) for statistical analysis and graphical representation.

Bicolor representative pictures

For representative photos of bicolor virus approach, brains infected with AAVrg-ef1a-DO-DIO-TdTomato-eGFP were incubated overnight at 4°C with rabbit anti-GFP (A-11122, Thermo Fisher Scientific) and rat anti-tdTomato (16D7, Kerafast) diluted 1:500 in a solution of 3% bovine albumin serum and 0.3% Triton X-100 prepared in PBS 1x. After primary incubation, the tissue was rinsed 3 times with PBS 1x and incubated at room temperature for 1.5h with goat anti-rabbit IgG H&L (Alexa Fluor® 488) and donkey anti-rat IgG H&L (Alexa Fluor® 555) diluted 1:500 in a solution of 0.25% Tween-20 prepared in PBS 1x. After staining procedures or simple slicing (injection or implantation site post-hoc confirmation), slices were rinsed 3 times in PBS 1x, mounted on glass slides and covered with mounting medium with DAPI and cover slides.

Rabies cell counting

In order to quantify monosynaptic inputs to D1-MSNs of the NAc the retrograde trans-synaptic labeling capability of the rabies virus was preferred over standard AAV labeling. Initially, D1-Cre mice were infected with AAV8-hSyn-Flex-TVA-P2A-GFP-2A-oG in the lateral shell of the NAc and after a 4-week waiting period they were injected with EnvA-RVdG-mCherry. Rabies expression was allowed for 7 days before sacrifice. Similarly to bicolor cell counting (see above), brain slices were collected from +2.50mm to -1.00mm to cover the entire length of the insular cortex. After image acquisition with Axioscan.Z1 slide scanner, image processing and cell counting was performed using Zen 3 (Blue version) software built-in features.

For every brain slice bregma coordinates and the insular cortex area were measured in accordance with standard anatomical references and the help of mouse brain atlases (Franklin & Paxinos, 2008). Cell counting was performed counting positive cells inside identified insular cortex boundaries. Subsequently cellular density index was calculated in Excel by dividing the number of positive cells by the area of the IC. Every slice measured was then pulled into one of 7 segments of 0.50mm length (ranging from +2.25mm to -0.75mm) based on their bregma coordinates to provide a rostro-caudal gradient of cellular density. Cellular density was also measured by using standard IC subdivisions.

Rabies representative pictures

Brains infected with AAV8-hSyn-Flex-TVA-P2A-GFP-2A-oG and EnvA-RVdG-mCherry were incubated overnight at 4°C with rabbit anti-mCherry (PA5-34974, Thermo Fisher Scientific) diluted 1:500 in a solution of 3% bovine albumin serum and 0.3% Triton X-100 prepared in PBS 1x. After primary incubation, the tissue was rinsed 3 times with PBS 1x and incubated at room temperature for 1.5h with goat anti-rabbit IgG H&L (Alexa Fluor® 555) diluted 1:500 in a solution of 0.25% Tween-20 prepared in PBS 1x.

In situ hybridization using RNAscope.

Fluorescent in situ hybridization was performed using the ACDBio V2 RNAScope kit (Advanced Cell Diagnostics). The following products were used: RNAscope Multiplex Fluorescent Reagent Kit V2 (cat. no. 323110), Fluorescent Multiplex Detection Reagents (cat. no. 323110), probes for td-Tomato (cat. no. 317041 C-2) and Drd1 (cat. no. 461901), and the PerkinElmer TSA Plus Fluorescence Palette Kit (cat. no. NEL760001KT). The Brains were perfused with cold saline solution followed by overnight fixation in paraformaldehyde 4% and immersed in a series of sucrose baths 10%, 20% and 30% for 3 consecutive days. 12 µm-tick coronal sections were prepared using a cryostat and incubated at room temperature for 1 hour. Sections were then fixed with 4% PFA for 15 min and processed for the staining according to the manufacturer's instructions, using the RNAscope Multiplex Fluorescent Reagent Kit v2 Assay (Advanced Cell Diagnostics) for fixed frozen tissue. Briefly, sections were dehydrated using 50%, 70% and 100% successive baths. td-Tomato (cat. no. 317041-C2) and Drd1 (cat. no. 461901-C1) probes were then incubated on sections for 2 hours at 40°C and processed for amplification steps. Finally, sections were counterstained with DAPI for 10 minutes, mounted with PVA-DABCO medium and left to dry overnight before imaging.

Behavior

Free social interaction test:

The animals were placed in a new home cage (35 cm x 19 cm x 13 cm), after a few minutes of habituation we introduced the stimuli: a juvenile mouse conspecific (post-natal age range P21-P35), unanimated object, or a CD1 conspecific. After 15 minutes of free interaction, the animals were separated and returned to the original home cage. During direct free interaction, we quantified prosocial, aggressive and defensive interactions between the experimental mouse and a conspecific juvenile.

Approach/avoidance test (day 2):

After Free social interaction test (day 1) exactly as described before. We positioned the animals in a corridor arena (60 cm x 15 cm x 30 cm) wherein on one of the sides we put an empty enclosure (7 cm x 11 cm x 30 cm) with vertical metal bars (1 cm distance between them), allowing the mice to interact through it. After 10 min of exploration, we replace the enclosure with another one that contain the same stimuli they interacted with the day before. Then we let them interact for another 10 minutes. For miniscope experiments, we performed one session per day for three consecutive days. The animals were exposed to object, 24h after juvenile and 24h after to CD1.

Fos CreERt2 mice:

Prior to the free interaction test and after the viral injections, CreERt2 mice were habituated 15 minutes for 5 consecutive days in a new home cage (35 cm x 19 cm x 13 cm) prior to the behavioral experiments, each “habituation cage” was specific for one animal during all sessions. At the end of each habituation session, they were injected intraperitoneally with a saline solution (1mL/Kg) according to the protocol described by Ye et al. 2016. The day of the test, after an initial period of 15 minutes of habituation, they performed a direct free interaction with a conspecific (CD1, juvenile or object) for 15 minutes. After that, they received an intraperitoneal injection of 4-OH Tamoxifen (10mg/Kg) to induce the Cre-recombinase expression. They were then left in their “habituation cage” for 4 hours to assure the level of cre expression is specific to the social interaction time-window (Ye et al. 2016). After this period, they were put back in their home cages.

In-vivo optogenetic stimulation:

The animals were injected with channelrhodopsin in AIC and mCherry in LNAc as previously described. During day 1 we deliver two different protocols of optogenetic stimulation: 1 Hz or 10 Hz in the ipsilateral hemisphere, then after the ipsilateral stimulation, in the

contralateral hemisphere, we delivered 0.1 Hz as a control. The 1 Hz stimulation consists of continuous stimulation of 450 pulses at 1 Hz (1ms pulses, 10-12mW). 10 Hz stimulation consists of a burst of 15 pulses at 10Hz (1ms pulses, 10-12mW) each 0.6 s, 150 times. 0.1 Hz stimulation consists of continuous stimulation of 60 pulses each 10 s (1ms pulses, 10-12mW). We deliver the protocol in a novel home cage (35 cm x 19 cm x 13 cm). The next day we prepared the animals for patch-clamp whole-cell recordings.

Optogenetic stimulation during free interaction

The animals were injected with channelrhodopsin in AIC and mCherry in LNAc as previously described. During day 1, we performed the free social interaction test following an optogenetic stimulation. We deliver a burst of 15 pulses at 10Hz (1ms pulses, 10-12mW) each 0.6 s, 150 times in an open loop manner, during each bout of interaction: nose-nose, nose-body and approach. Day 2, corresponds to the same approach/avoidance test previously described above. After day 2 approach/avoidance test, the animals were prepared for ex-vivo electrophysiology.

Electrophysiology

Ex-vivo patch clamp recordings

We prepared 250 µm thick coronal slices containing LNAc. Slices were kept in artificial cerebrospinal fluid containing 119 mM NaCl, 2.5 mM KCl, 1.3 mM MgCl2, 2.5 mM CaCl2, 1.0 mM NaH2PO4, 26.2 mM NaHCO3, and 11 mM glucose, bubbled with 95% O2 and 5% CO2. Slices were maintained 30 min in bath at 30°C and then at room temperature. Whole-cell voltage-clamp recording techniques were used (37°C, 2–3 ml/min, submerged slices) to measure the holding currents and synaptic responses. The internal solution contained 130 mM CsCl, 4 mM NaCl, 2 mM MgCl2, 1.1 mM EGTA, 5 mM HEPES, 2 mM Na2ATP, 5 mM sodium creatine phosphate, 0.6 mM Na3GTP, and 0.1 mM spermine.

Access resistance was monitored by a hyperpolarizing step of -4 mV at each sweep, every 10s. The cells were recorded at the access resistance from 5 to 20 MΩ for MSN. Data were excluded when the resistance changed more than 25% across the recording. Synaptic currents were evoked by optogenetic stimulation at 0.1 Hz and 1-3 ms of duration. The experiments were conducted in the presence of GABAA receptor antagonist picrotoxin (100 mM); the AMPAR-EPSCs were pharmacologically isolated by application of the NMDAR antagonist D-APV (50 mM) and NMDAR EPSCs were recorded at +40 mV in presence of the AMPAR blocker NBQX (10 mM). Representative example traces are shown as the average of 15–20 consecutive EPSCs typically obtained at each potential. The rectification index of AMPARs is the ratio of the chord conductance calculated at negative potential (-60

mV) divided by the chord conductance at positive potential (+40 mV). The Synaptic responses were collected with a Multiclamp 700B-amplifier (Axon Instruments), filtered at 2.2 kHz, digitized at 10 Hz, and analyzed using Igor Pro 6.3 and 8.0 software (Wavemetrics).

Behavioral and data analysis

Free social interaction

The animals were tracked using DeepLabCut with different models built for object and experimental, juvenile and CD1 animal to detect nose, body and tail of each tracked subject (corresponding to left, center and right side of the object). All the coordinates of the tracked position by DeepLabCut were calibrated by using the size in cm of the cage and corrected by using the body of the experimental mice as the origin coordinates and the nose of the experimental mice aligned to the y-axis. All the tracked position of the social stimulus was then plotted relative to the position of the experimental mice. Coordinates with a likelihood lower than 95%, defined by DeepLabCut, were replaced by interpolation.

The distance and the angle between the experimental and the stimulus position were reported for each frame and time distribution probability was computed. For each frame, the corresponding calcium activity was reported and analyzed depending on the proximity and the angle in the same way as the time distribution of the stimuli position.

To extract contact events, a threshold of 5cm proximity and 0.2 to 2 seconds duration was applied regarding the position of the experimental and stimuli nose and base of the tail.

Classifier approach

The valence of each contact event was defined by the prediction of a SVM trained to classify the type of social stimuli at the origin of the latent embedding obtained from a VAE trained to reconstruct contact with juvenile animal (Extended data 4). More precisely, input data was obtained by the sum of coordinates throughout the contact by taking each timepoint as a spatial and temporal egocentric reference. A VAE was trained to minimize the reconstruction error of 70% of the contact with juvenile animal and tested with the remaining 30% held-out contact. The trained VAE was then used to encode all the contact of juvenile and CD1 animal in a latent space of 128 dimensions. Then the dimensionality was reduced by using UMAP technique for visualization or a classifier was built by using SVM to predict the stimuli involved in each contact (Extended data 5). To assess eventual overfitting, prediction accuracy was obtained based on 1 hold-out 5-fold cross-validation and was similar with or without 1 hold-out validation (eg. 1 classifier created for each contact by excluding the contact tested during the training). Peri-event time histogram was then made

by aligning and centering human manual annotation of nose contact and aggression with the contact classified by the SVM and the occurrence was normalized by z-score. Contact predicting prosocial experience coming from juvenile stimuli was then defined as affiliative and contact predicting aversive interaction coming from CD1 stimuli was defined as antagonistic.

Acquisition calcium recordings

Calcium recordings were performed using an nVista miniaturized epifluorescent microscope (Inscopix). All recordings were made at 10 frames per second. Optimal field of view was determined during habituation 1–2 days before starting the recordings. LED intensities (0.1–2 mW) and gain (1–5 x) were optimized per animal for sufficient signal-to-noise while minimizing fluorescent bleaching. The recordings were synchronized by a TTL signal from Ethovision acquisition software through a mini I/O box into the SYNC-port on Inscopix data acquisition box. The signal was triggered from the beginning till the end of each acquisition trial.

The acquired images were spatially downsampled 4 x, cropped, and motion-corrected using Inscopix Data Processing Software. Identification of regions of interest (ROIs) was then done using Constrained Nonnegative Matrix Factorization for microendoscopic data (CNMF-E)[20]. We used the CNMF-E tools neuron.merge, neurons_dist_corr(), neuron.merge_hig_corr(), neuron.merge_close_neighbors and neuron.quickMerge, to automatically remove potential noise ROIs obtained from Ruud van Zessen et al., 2021. ROIs with poor signal/noise quality were also excluded. Furthermore, we identified the total surface area of each ROI and checked the smallest ROIs manually to assess whether or not they could be considered as neurons. Following quality control, the temporal ('C_raw' label in CNMF-E) and spatial ('A' label in CNMF-E) data were used for further analyses. For the neuronal tracking of the cells across sessions, we obtained the spatial footprints and then we used the probabilistic method CellReg [21] to track the cells across prosocial and aversive experiences.

Analysis calcium activity

Time course of calcium activity was normalized by z-score. To define response of each neuron to the different stimuli, total time of significant increased calcium activity (>1.96 z-score) was compared between stimuli exposure and baseline.

Heatmaps of calcium activity were obtained by averaging the neuronal activity recorded for each x and y position with 5mm resolution of stimuli tracked with experimental mice as egocentric reference and then filtered with a 2 cm2 convolution.

PETH analyzes were then performed and neuronal activity was aligned on the center of the previously defined contact events. Decoding approach was used to create a model and attempt to reveal whether particular information is representative of calcium neuronal activity to predict valence of contact events (affiliative and antagonistic) defined previously. Based on PETHs of calcium activity from recorded neurons around a time window from -10sec to +10sec surrounding each event, multiple features were analyzed. To obtain these features, the probability distribution of amplitude of activity and duration (expressed in ratio of total time) of significant increased activity (>1.96 z-score) was computed and the following properties of each distribution were extracted: mean, median, coefficient of variation, skewness and kurtosis. The number of time bouts as well as the total duration in significant increased activity was also computed. The features were normalized by using z-score and by rescaling the values. Then a classifier was built by using k-nearest neighbor 1 hold-out 5-fold cross-validation (1 classifier created for each neuron of each contact by excluding the neuron tested during the training).

By using this classifier model, the posterior probability that the calcium activity during a given event is associated with each social contact (affiliative or antagonistic) was then calculated.

References

Acknowledgments

We thank Manuel Mamelli and Christian Lüscher for their suggestions in the manuscript. P.E. is supported by the Swiss Government Excellence Scholarship (FCS) for PhD Studies Grant ESKAS-Nr: 2017.0922. C.B. is supported by the Swiss National Science Foundation and by Synapsis Foundation.

Author Contributions

P.E. and C.B. conceived the project. C.B. and P.E. wrote the manuscript with collaboration of B.G. All the experiments were performed by P.E. The code and the analytical method for the classifier approach in Figure 2 and Extended figure 4 and 5 were developed by B.G. Anatomical tracing experiments were performed by P.E. with assistance of M.L. and V.T. Cell counting was performed by M.L and V.T. All the analyses and statistics were performed by P.E., with assistance of B.G. for Figures 1 and 2. P.E. made the figures.

Competing interests

The authors declare no competing interests.

References

1. Padilla-Coreano, N., Tye, K. M. & Zelikowsky, M. Dynamic influences on the neural encoding of social valence. *Nat Rev Neurosci* **23**, 535–550 (2022).
2. Gunaydin, L. A. *et al.* Natural Neural Projection Dynamics Underlying Social Behavior. *Cell* **157**, (2014).
3. Solié, C. *et al.* Superior Colliculus to VTA pathway controls orienting response and influences social interaction in mice. *Nat Commun* **13**, (2022).
4. Solié, C., Girard, B., Righetti, B., Tapparel, M. & Bellone, C. VTA dopamine neuron activity encodes social interaction and promotes reinforcement learning through social prediction error. *Nat Neurosci* **25**, (2022).
5. Chen, P. & Hong, W. Neural Circuit Mechanisms of Social Behavior. *Neuron* **98**, 16–30 (2018).
6. Hung, L. W. *et al.* Gating of social reward by oxytocin in the ventral tegmental area. *Science (1979)* **357**, (2017).
7. Hu, R. K. *et al.* An amygdala-to-hypothalamus circuit for social reward. *Nat Neurosci* **24**, 831–842 (2021).
8. Soares-Cunha, C., Coimbra, B., Sousa, N. & Rodrigues, A. J. Reappraising striatal D1- and D2-neurons in reward and aversion. *Neurosci Biobehav Rev* **68**, 370–386 (2016).
9. Steinberg, E. E. *et al.* Positive Reinforcement Mediated by Midbrain Dopamine Neurons Requires D1 and D2 Receptor Activation in the Nucleus Accumbens. *PLoS One* **9**, e94771 (2014).
10. Gerfen, C. R. & Surmeier, D. J. Modulation of Striatal Projection Systems by Dopamine. *Annu Rev Neurosci* **34**, 441–466 (2011).
11. Francis, T. C. *et al.* Nucleus Accumbens Medium Spiny Neuron Subtypes Mediate Depression-Related Outcomes to Social Defeat Stress. *Biol Psychiatry* **77**, 212–222 (2015).
12. Yang, H. *et al.* Nucleus Accumbens Subnuclei Regulate Motivated Behavior via Direct Inhibition and Disinhibition of VTA Dopamine Subpopulations. *Neuron* **97**, 434-449.e4 (2018).
13. Yuan, L., Dou, Y.-N. & Sun, Y.-G. Topography of Reward and Aversion Encoding in the Mesolimbic Dopaminergic System. *The Journal of Neuroscience* **39**, 6472–6481 (2019).
14. Gogolla, N. The insular cortex. *Current Biology* **27**, (2017).
15. Molnar-Szakacs, I. & Uddin, L. Q. Anterior insula as a gatekeeper of executive control. *Neurosci Biobehav Rev* **139**, 104736 (2022).
16. Xing, B., Mack, N. R., Zhang, Y.-X., McEachern, E. P. & Gao, W.-J. Distinct Roles for Prefrontal Dopamine D1 and D2 Neurons in Social Hierarchy. *The Journal of Neuroscience* **42**, 313–324 (2022).
17. Mathis, A. *et al.* DeepLabCut: markerless pose estimation of user-defined body parts with deep learning. *Nat Neurosci* **21**, 1281–1289 (2018).
18. Bellone, C. & Lüscher, C. Cocaine triggered AMPA receptor redistribution is reversed in vivo by mGluR-dependent long-term depression. *Nat Neurosci* **9**, 636–641 (2006).
19. Citri, A. & Malenka, R. C. Synaptic Plasticity: Multiple Forms, Functions, and Mechanisms. *Neuropsychopharmacology* **33**, 18–41 (2008).
20. Zhou, P. *et al.* Efficient and accurate extraction of in vivo calcium signals from microendoscopic video data. *Elife* **7**, (2018).
21. Sheintuch, L. *et al.* Tracking the Same Neurons across Multiple Days in Ca2+ Imaging Data. *Cell Rep* **21**, 1102–1115 (2017).

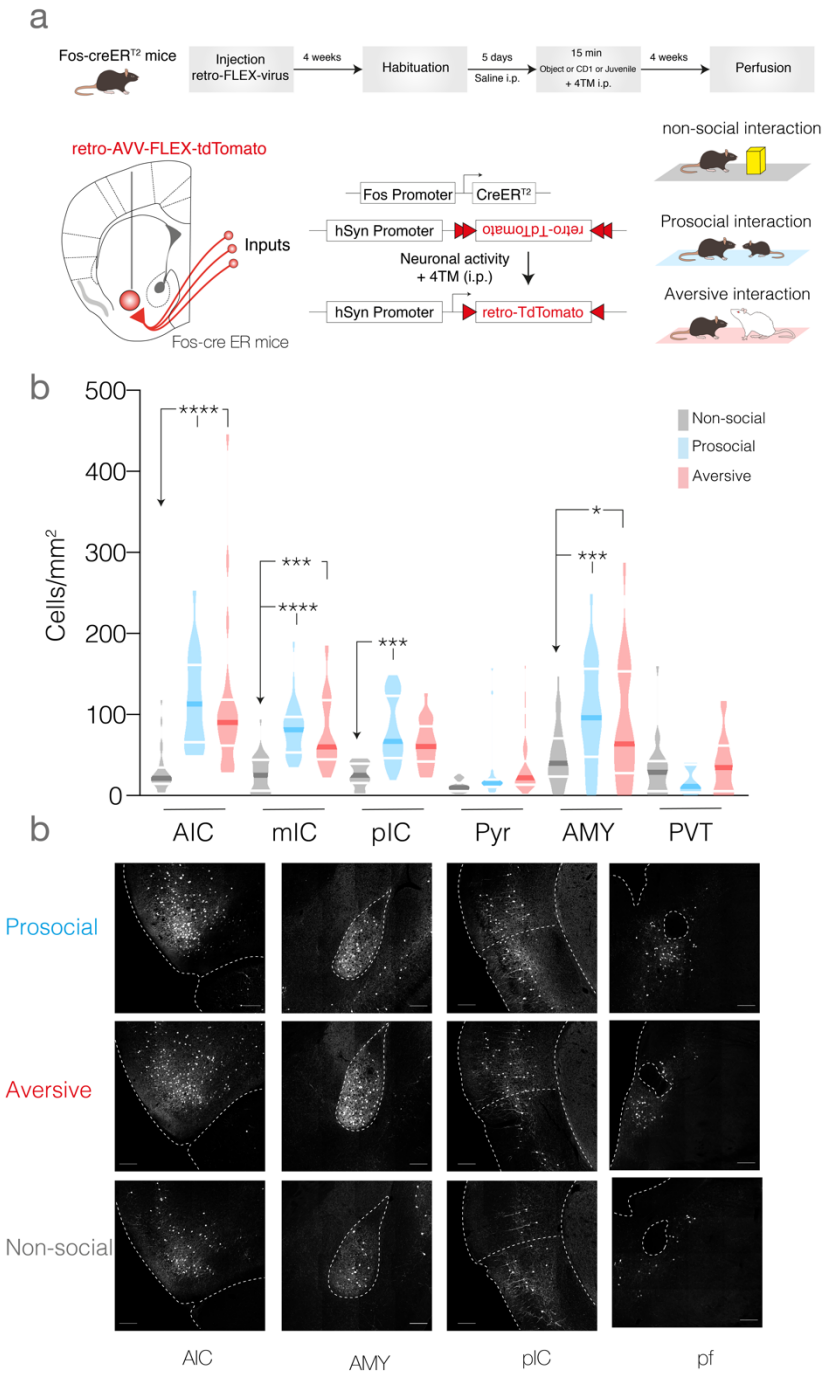

Extended Data Fig. 1. Anatomical characterization of LNAc active inputs. a, Schema of experimental protocol, showing the viral injection and the transgenic construct after activation by 4-OH tamoxifen injection. **b**, Quantification of cell densities from the main brain regions projecting to LNAc, represents the overall active inputs during free social interaction. **d**, Representative pictures of active neurons in different brain regions, AIC: anterior insular cortex, AMY: Basolateral amygdala, pIC, Posterior insular cortex, pf: Parafasicular thalamic nucleus. One-way ANOVA was used as statistical test. For AIC: ****= p<0.0001, mIC: ****= p<0.0001, ***= p=0.0002, pIC: ***= p=0.0001. AMY: *= p=0.0378, ***= p=0.0004. n=4 per condition (prosocial, aversive, non-social).

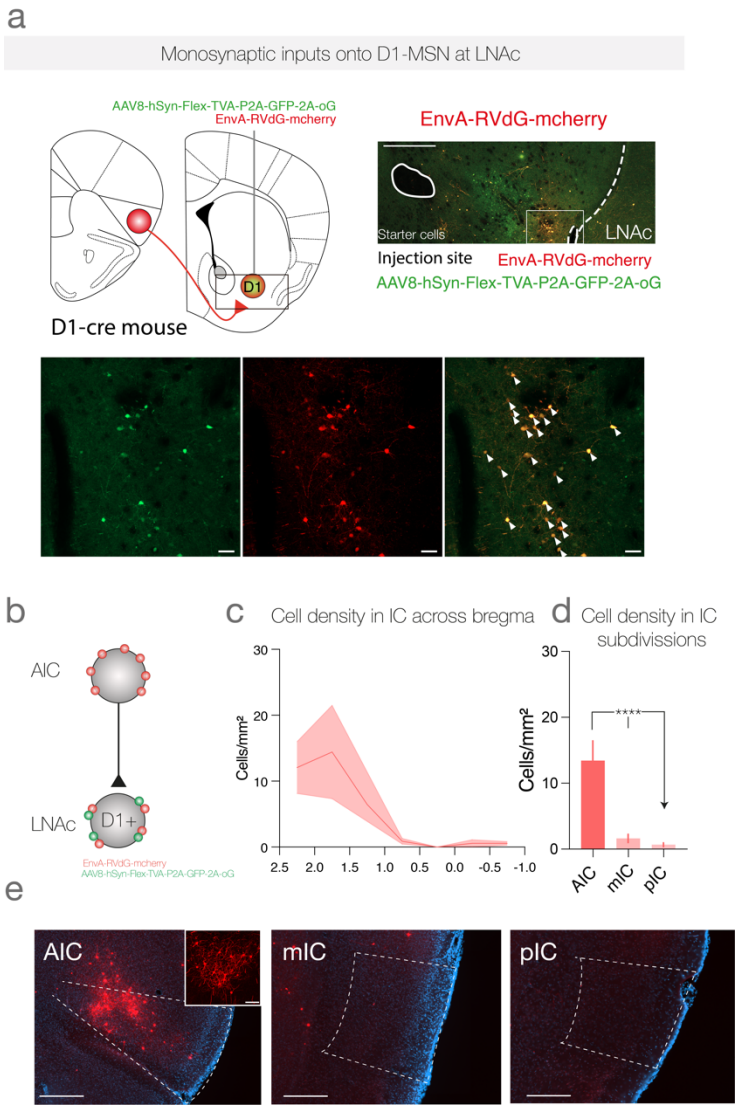

Extended Data Fig. 2. Anatomical characterization of AIC monosynaptic inputs onto D1-MSN of LNAc. a, Left, schematic showing the viral injection (scale 500 µm) and at the right panel the representative picture of the injection site. Below, magnification of injection site, scale 50 µm. **b**, schematic illustrating the mechanism of rabies viral expression. **c**, Cell densitiy across the rostro-caudal axis of mCherry positive neurons. **d**, same quantification but separated across the different insular subdivision, AIC: anterior insular cortex, mIC, medial insular cortex and pIC, posterior insular cortex. One-way ANOVA was used as statistical test, ****p<0.0001. **e**, Representative pictures in each subdivision of insular cortex scale 500 µm, in AIC, the small picture represent a magnification with a confocal microscope, scale 100 µm, n=3.

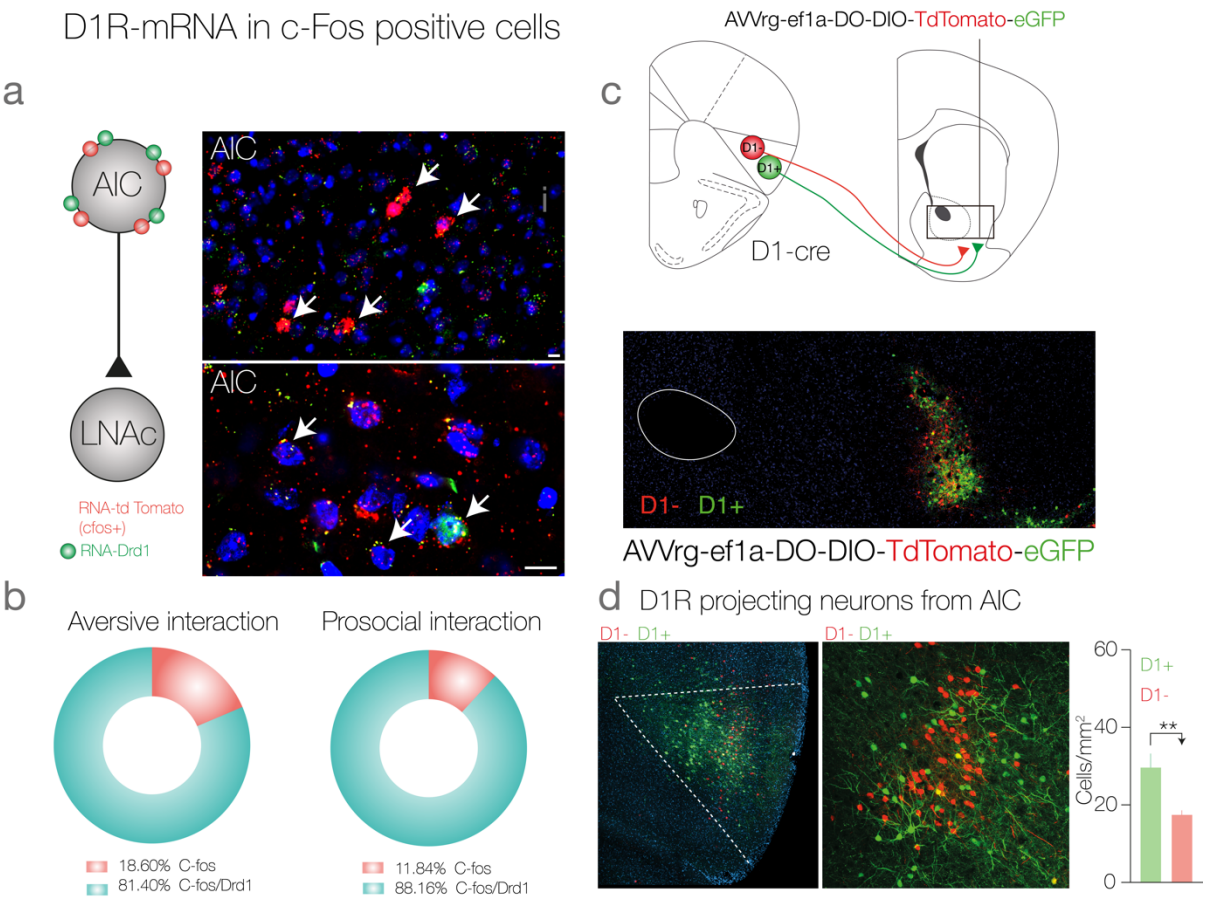

Extended Data Fig. 3. Cellular characterization of AIC-LNAc pathway. a, hybridization in situ for mRNA of D1R and td-Tomato, showing a high correspondence between c-fos positive cells (mRNA td-Tomato) and D1R mRNA, scale 10 µm. n=2 for aversive and n=3 for prosocial. **b**, most of the neurons colocalize for mRNA of td-tomato (c-fos signal) and D1R. **c**, schematic of viral injection where we employed a bicolor retro virus that will turn green in presence of cre-recombinase, and it will remain red in absence of it, scale 500 µm. Below the representative picture of site of injection. Right panel, representative image of AIC illustrating the D1R projecting neurons subpopulation and its quantification in the AIC. **d**, Left, Picture of AIC showing the D1 positive neurons in green and D1 negative in red. Right, a magnification of AIC showing in detail the proportion of D1 positive and negative cells. The histogram represents the quantification of D1 positive and negative cells in AIC, unpaired t-test, **= p=0.0091, n=4.

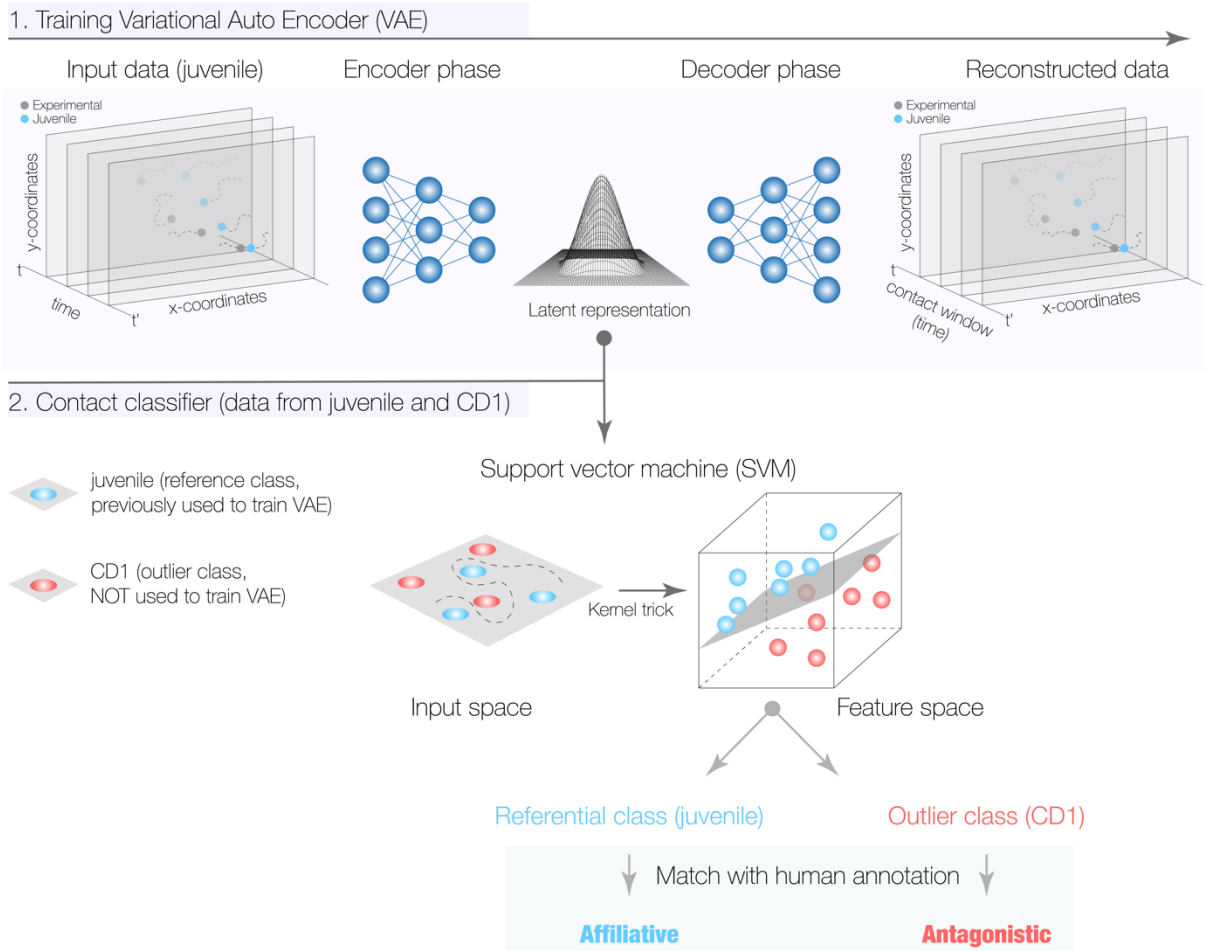

Extended Data Fig. 4. Behavioral classifier. a, Training of a variational autoencoder (VAE) by using coordinates data of each contact with juvenile stimuli (prosocial experience) used as referential class. b, Training of contact classifier by using SVM algorithm with latent representation of VAE from contact with juvenile stimuli (prosocial experiences) and CD1 stimuli (aversive experiences). Accuracy of classifier for each class and matching of predicted class with human manual annotation were made and shown in Figure 2. Contact classified in referential class is defined as affiliative and contact classified in outlier class is defined as antagonistic.

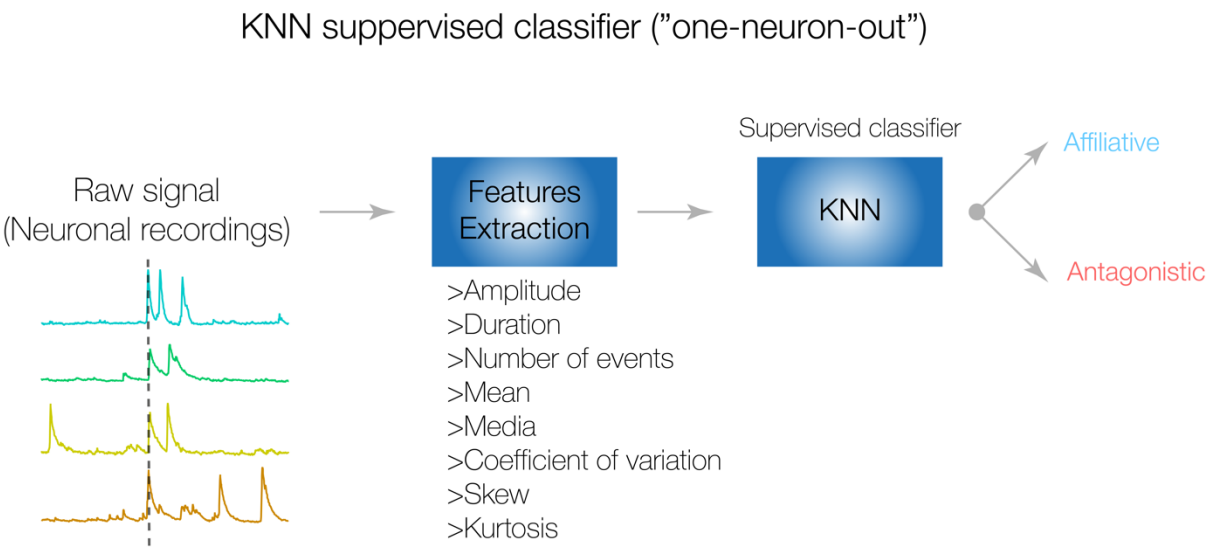

Extended Data Fig. 5. Classifier for calcium activity of individual neurons. One-neuron-out training by using KNN algorithm with features obtained from calcium activity of individual neurons during affiliative and antagonistic contact. For each neuron n analyzed, a classifier was trained by using all the neurons except the neuron n analyzed and then the neuron n analyzed was tested with the classifier to predict the probability of coming from affiliative or antagonistic contact.

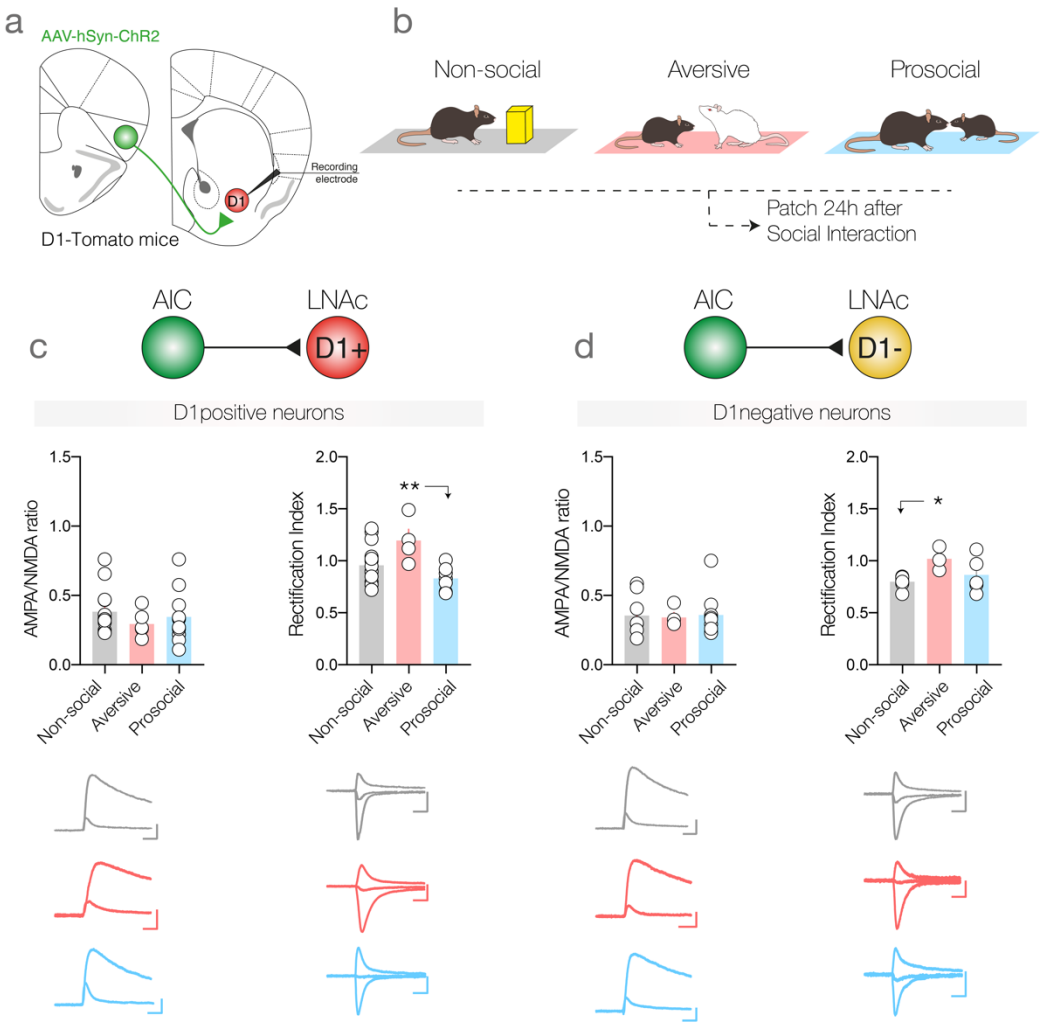

Extended Data Fig. 6. hSyn promoter channelrhodopisn expression in AIC neurons does not elicit synaptic plasticity after social interaction. a, scheme of viral injection and patch recordings. **b**, Protocol of free social interaction **c**, AMPA/NMDA ration, for non-social versus juvenile p>0.9999, non-social versus aversive p=0.7779. Right, rectification index in D1-MSN, for non-social vs juvenile p=0.3941, non-social versus aversive p=0.0747, **= p=0.0095, showing the lack of plasticity after social interaction. **d**, AMPA/NMDA ratio (p>0.9999 in all conditions) and rectification index in D1 negative-MSN, for non-social versus juvenile p>0.9999 and *= p=0.0405, showing the lack of plasticity after social interaction. Below the representative traces for each group. Scale 10ms/100pA. One-way ANOVA was used as statistical test.

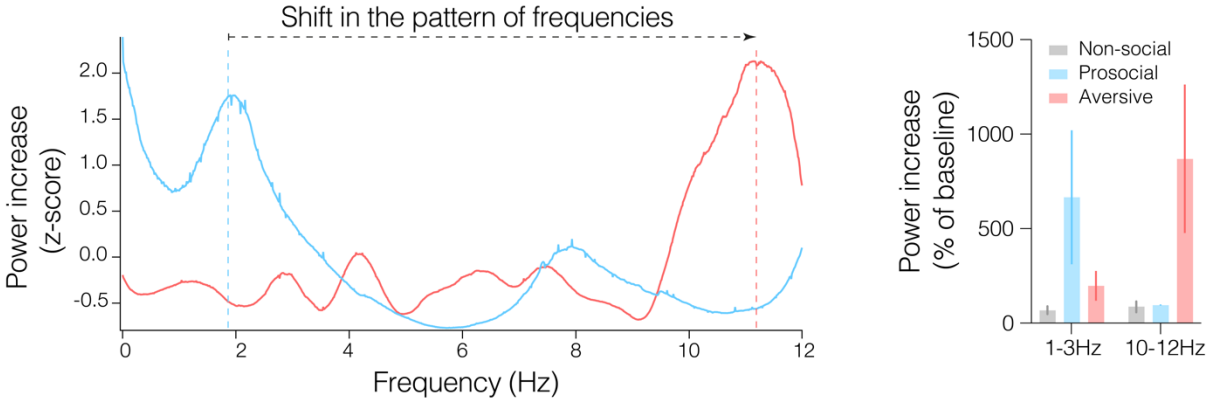

Extended Data Fig. 7. Prosocial and aversive social experiences elicit different patterns of activity in D1-AIC. Left, the schematic shows the shift in the frequencies for prosocial and aversive experiences from calcium activity. Right, bar plot showing for prosocial interaction a higher contribution of low frequencies (1-3 Hz) and for aversive experiences an increase in higher frequencies (10-12 Hz).